

REPEATED LOAD TRIAXIAL TESTING FOR QUALITY ASSESSMENT OF UNBOUND GRANULAR BASE COURSE MATERIALS

Magnusdottir, B.

Engineering Research Institute, University of Iceland, IS-107 Reykjavik, Iceland; brynhma@hi.is

Erlingsson, S.

Engineering Research Institute, University of Iceland, IS-107 Reykjavik, Iceland; sigger@hi.is

1 INTRODUCTION

One of the current main research topics in highway engineering is the analytical design of flexible pavement structures. A fundamental requirement for an analytical approach towards a pavement design is a proper understanding of the mechanical properties of the constituent materials. The granular base and subbase layers (the unbound granular materials, UGM) in a flexible pavement play an essential role in the overall structural performance of the pavement. For better understanding, tests where in-situ stress conditions and traffic load are adequately simulated are needed. Repeated load triaxial testing (RLTT) is one such method. The most important parameters evaluated in RLTT are the stiffness characteristics of the material as well as the ability to withstand the accumulation of permanent deformation during pulsating loading.

2 CHARACTERISTICS OF UGM

Figure 1 illustrates the general stress regime experienced by an unbound base course element in a pavement structure as the result of a moving wheel load within the plane of the wheel track. Due to the wheel load, pulses of vertical and horizontal stress, accompanied by a double pulse of shear stress with a sign reversal, affect the element (Brown, 1996).

UGM shows complex nonlinear elastic-plastic behaviour during external loading where wheel loading is adequately simulated. The material response can be expressed in terms of the strains where the total strains are divided into elastic strains and plastic strains:

$$\varepsilon^{tot} = \varepsilon^{el} + \varepsilon^{pl} \quad (1)$$

Usually in a road structure the largest part of the strains is caused by the elastic response with only a small part due to plastic behaviour. In the laboratory where this is simulated the elastic

response reflects the stiffness characteristics of the specimen but the plastic strains gives information about the permanent deformation behaviour of the specimen. During triaxial testing of a cylindrical specimen the confining pressure is equal to the radial stress and $\sigma_2 = \sigma_3$. The axial stress σ_1 on the other hand is varied to simulate the stress situation caused by the wheel loading.

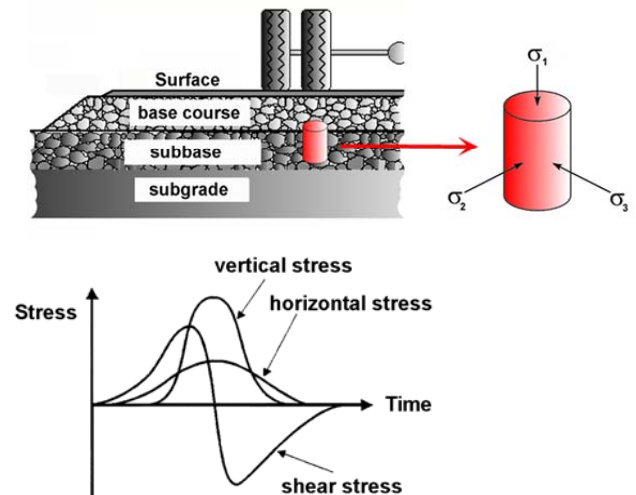


Figure 1. Stresses in a UGM layer. a) Typical pavement structure and stresses, b) induced stresses in a pavement element due to moving wheel load.

The stress regime in RLTT can be expressed by introducing two stress invariants: the mean stress level p and the deviatoric stress q , which for the the case where $\sigma_2 = \sigma_3$, becomes

$$p = \frac{1}{3}(\sigma_1 + 2\sigma_3) \quad \text{and} \quad q = \sigma_1 - \sigma_3 \quad (2)$$

In a similar way strain invariants can be introduced. The volumetric strain ε_v and deviatoric strain ε_q , are defined in RLTT as

$$\varepsilon_v = \varepsilon_1 + 2\varepsilon_3 \quad \text{and} \quad \varepsilon_q = \frac{2}{3}(\varepsilon_1 - \varepsilon_3) \quad (3)$$

in which ε_1 and ε_3 are the resilient axial strain and radial strain respectively, where it has been assumed in a comparable way as for the stresses that $\varepsilon_2 = \varepsilon_3$.

The stresses and strains are now interconnected through the material properties and the elastic response of the material can be expressed according to Hooke's law as a diagonal matrix:

$$\begin{bmatrix} \varepsilon_v \\ \varepsilon_q \end{bmatrix} = \frac{1}{E} \begin{bmatrix} 3(1-2\nu) & 0 \\ 0 & 2(1+\nu) \end{bmatrix} \begin{bmatrix} p \\ q \end{bmatrix} \quad (4)$$

where E and ν are the material stiffness modulus (resilient modulus) and Poisson's ratio respectively, defined as:

$$E = \frac{q}{\varepsilon_1} \quad \text{and} \quad \nu = -\frac{\varepsilon_3}{\varepsilon_1} \quad (5)$$

The stiffness modulus is stress dependent but the Poisson's ratio is not, or at least is to a much less extent and can be treated in many engineering applications as a constant. A number of relationships exist to describe the stress dependency of the stiffness moduli. One of the most common and also one of the simplest is the $k - \theta$ expression (Gomes-Correia et al., 1999)

$$E = k_1 \left(\frac{3p}{p_a} \right)^{k_2} \quad (6)$$

where k_1 and k_2 are experimentally determined constants and p_a is a reference pressure, $p_a = 100$ kPa.

By introducing equation (6) into (4) it is obvious that the stresses and the strains are interconnected in a nonlinear relationship, which can be written in matrix form as

$$[\varepsilon] = [C(p)][\sigma] \quad (7)$$

in which $[\varepsilon]^T = [\varepsilon_v, \varepsilon_q]^T$ and $[\sigma]^T = [p, q]^T$ and $[C(p)]$ is the compliance matrix.

To determine the stress strain relationship experimentally, and therefore the k_1 , k_2 and ν , a number of measurements is needed to cover the actual range of mean stresses p and deviatoric stresses q caused by different weights of the axle loads of the traffic.

3 TESTING EQUIPMENT AND PROCEDURE

For the RLTT a Constant Confining Pressure method (CCP method) has been used, in accordance with CEN standard prEN 00227413 and SHRP protocol P46 (CEN pr ENV 00227413, 1997; AASHTO T294-92 I, 1992). A 150 mm diameter specimen with a height of 300 mm was used. With this equipment, material with grain sizes up to 30 mm can easily be tested. The material is compacted according to the Proctor compaction method, in a split cylinder lined with a

rubber membrane, usually up to a level corresponding to either Standard or Modified compaction energy (see figure 2). The response of the specimen is measured by four Hall effect displacement transducers, three of which measure the vertical strains over the middle third part of the specimen height located 120° apart from each other, and the fourth is used to measure the radial strains in the middle of the specimen height.



Figure 2. Preparation of the specimen. a) Fully compacted specimen in the split cylinder; the outer part of the anchors can be seen sticking out of the cylinder. b) A specimen with the mounted displacement transducers.

The testing procedure was divided into two phases, a conditioning phase and a testing phase. During the conditioning phase 20,000 symmetric haversine load pulses were applied with the frequency of 5 Hz to stabilize the response from the specimen. Thereafter 16 different stress paths were applied to estimate the specimen's response. During each stress path 100 symmetric haversine load cycles were applied with a rise time of 50 ms (total length of pulse 0.1 sec) followed by a 0.9 sec rest time. During the last ten load cycles data from the transducers as well as the axial load were collected to evaluate the specimen response (see figure 3).

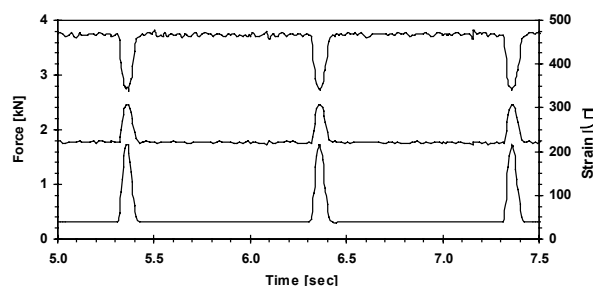


Figure 3. Measured response of the specimen. Three load pulses (the lowest curve) are shown and the strain response from one of the vertical transducers (the top curve) as well as the horizontal transducer (the middle curve). The vertical transducer shows compression during the load pulses and the horizontal one shows extension.

4 THE MATERIALS

The granular materials used in this research have all been used as base course or subbase materials. They are all of basaltic nature. Some parameters describing the material can be found in table 1 and the grain size distribution is given in figure 4.

Table 1. Percent fines, maximum size and optimum moisture content for the six materials tested.

Material	$D < 0.063$ mm [%]	D_{max} [mm]	w_{opt} [%]
Holabru (Fuller curve)	0.0	22.4	-
Holabru (HVS-curve)	3.9	25.0	5.6
Laxarberg (base course 1)	9.7	22.4	9.8
Daelisa (base course 2)	11.1	32.0	9.8
Daelisa (subbase 1)	7.2	32.0	10.8
Daelisa (subbase 2)	13.2	32.0	10.7

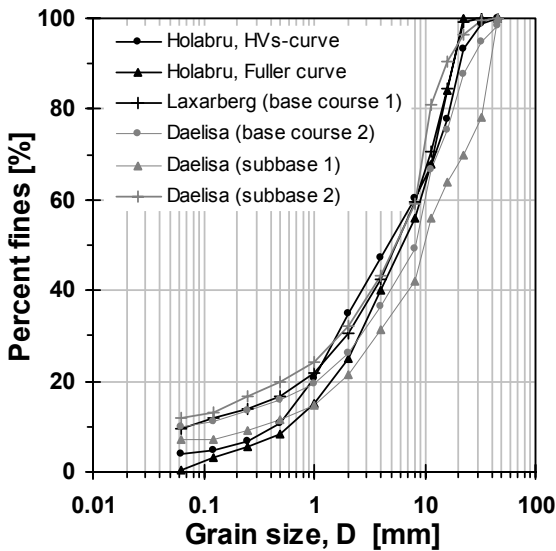


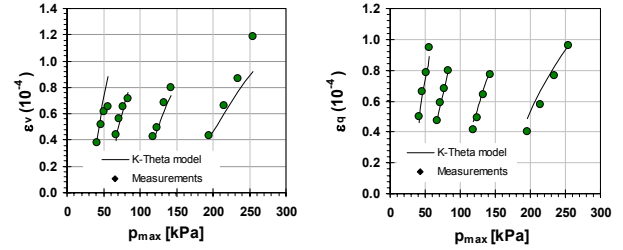
Figure 4. Grain size distribution for the six materials included in this study.

5 TEST RESULTS

Typical results from the RLTT are shown in figure 5 where the volumetric strain ε_v and deviatoric strain ε_q are plotted as functions of the mean stress level p . The data were further used to estimate k_1 and k_2 from equation (7) with the aid of the least square method, and these results are given as well in the figure.

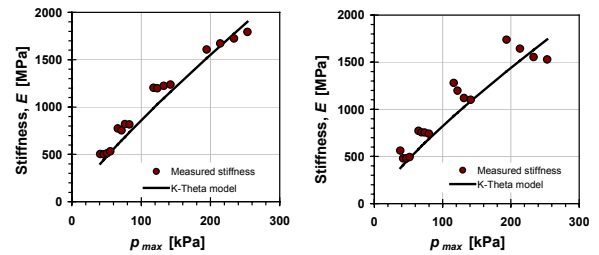
In figure 6 the measured stiffness is plotted along with the the results from the least square estimations of k_1 and k_2 from the $k - \theta$ expression. Two important factors affecting stiffness of UGM are the density of the specimen or the compaction effort used in the preparation process of the specimen and the moisture content or the degree of saturation.

Figure 5. Typical results from RLTT: comparison of measured and calculated strains. a) volumetric strain and b) deviatoric strain



versus the mean normal stress p .

Figure 6. Measured and calculated stiffness as a function of the mean normal stress p for the Daelisa material (subbase 1) see table 2, a) with



$k_1 = 336.7$ MPa and $k_2 = 0.85$ and b) with $k_1 = 337.8$ MPa and $k_2 = 0.81$. Both samples were compacted according to the Standard Proctor method, the former with $S_r = 77.5\%$, $w = 8.0\%$ and $\rho_{dry} = 2355.2$ kg/m³ and the latter $S_r = 72.8\%$, $w = 8.0\%$ and $\rho_{dry} = 2309.4$ kg/m³.

5.1 Influence of compaction on stiffness

The influence of the compaction effort on the stiffness was estimated for two materials. In general as a material is compacted the void ratio decreases. The void ratio has been found to be a good indicator of the dependence of stiffness on the compaction effort. It was found in some materials that stiffness was dependent on the compaction effort. This can be seen in figure 7. In figure 7a stiffness is shown as a function of the void ratio of the Holabru material with a Fuller curve, showing clearly that the stiffness values decreased as the void ratio increased and in figure 7b the stiffness is given as a function of the compaction energy effort used during the compaction phase for the Laxarberg material showing that as the energy used increased the stiffness increased. The increase in stiffness when going from a Standard Proctor energy (593 kJ/m³) up to a Modified Proctor compaction energy (2693 kJ/m³) was about 80%.

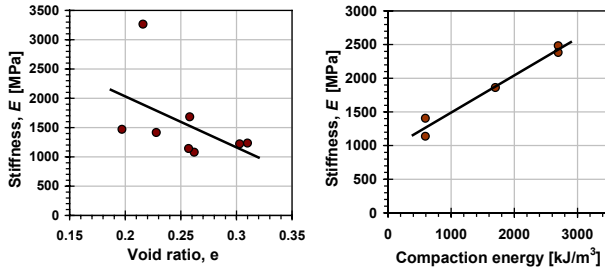


Figure 7. a) Stiffness as a function of void ratio for the Holabru material with a Fuller curve in table 1. All samples were compacted at a moisture content close to 5% (4.7% - 5.4%). b) Stiffness as a function of the compaction energy for the Laxarberg material in table 1. All samples were compacted at a moisture content close to 7% (6.6% - 7.6%). The results are based on the $k - \theta$ model with the mean stress level $p = 250$ kPa.

5.2 Influence of moisture on stiffness

Moisture content or degree of saturation influences the stiffness of UGM. To investigate this, three tests of the Holabru material with the HVS curve were compacted according to the Modified Proctor compaction method at three different moisture contents and tested in the RLTT equipment. The results are shown in table 2 and figure 8.

Table 2. Moisture content, degree of saturation, density and the coefficients k_1 and k_2 for three different tests of the Holabru material with HVS curve all made with the same compaction energy, corresponding to the Modified Proctor compaction method.

Test no	w [%]	S_r [%]	ρ_{dry} [kg/m ³]	k_1 [MPa]	k_2 [-]
1	3.7	54.6	2372	419.3	0.516
2	3.9	60.8	2391	683.2	0.410
3	5.3	85.4	2404	745.2	0.431

In table 2 one can see that the density increased as the moisture content increased. This was expected as the moisture content was lower than the optimum moisture content. Further, one can see that the k_1 value increased as the moisture content increased. In figure 8 the stiffness estimated for the $k - \theta$ model, equation (6), is plotted as a function of the mean stress level. However as can be seen in table 2 the dry density of the specimen increased as well. Therefore it is not clear if the increase in stiffness is due to increase in moisture content or because increased moisture results in increased compaction ability of the material resulting in higher dry density. A better indicator of the moisture influence on the stiffness behaviour is therefore degree of saturation.

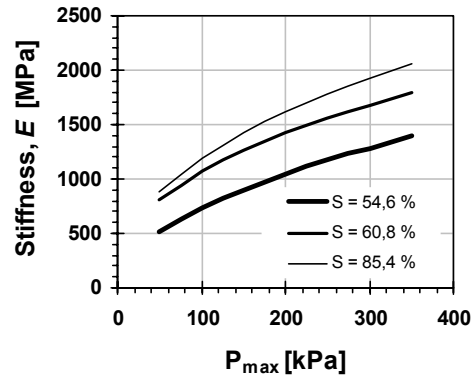


Figure 8. Stiffness as a function of the mean stress level for the Holabru material with HVS curve for three different values of the degree of saturation. All samples were compacted according to the Modified Proctor compaction method.

The material from Daelisa with 13.2% fines (subbase 2 in table 1) was also investigated. The test results are shown in figure 9 where stiffness is given as a function of the degree of saturation. The data points were obtained from the respective $k - \theta$ model (k_1 and k_2 values) where the mean stress level was chosen as $p = 250$ kPa. The results show that stiffness increased as the degree of saturation increased. However, as some critical point was exceeded stiffness started to decrease quite steeply. For the Daelisa material the turning point where the stiffness started to decrease was when the degree of saturation was around $S_r = 76 - 78$ %. When the degree of saturation exceeded 90% the stiffness was only about 43% of the highest stiffness value obtained at $S_r = 78$ %.

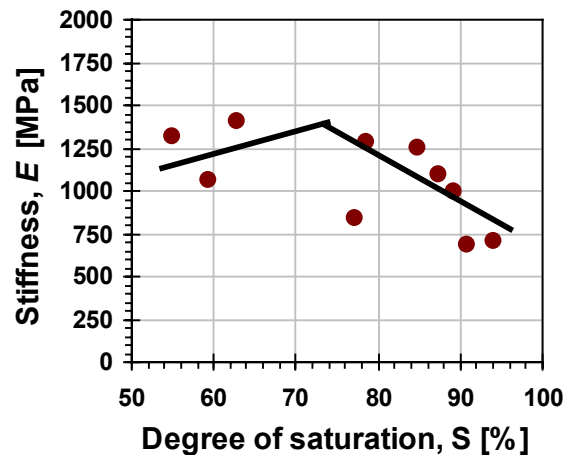


Figure 9. Stiffness as a function of degree of saturation for the Daelisa material (subbase 2) with 13.2 % content of fines. All samples were compacted according to the Standard Proctor compaction method. The results are based on the $k - \theta$ model with the mean stress level $p = 250$ kPa.

5.3 Influence of contents of fines on stiffness

One material with different contents of fines has been tested. The details are given in table 3.

Table 3. Contents of fines, maximum aggregate size, optimum water content, maximum density and the water content when tested for the Daelisa material. All samples are made with the same compaction energy, corresponding to the Standard Proctor compaction method.

Test no	$D < 0.063$ mm [%]	D_{max} [mm]	ρ_{dry} [kg/m ³]	w_{opt} [%]	w [%]
1	7.2	32	2279	10.8	8.1
2	11.1	32	2234	9.8	7.8
3	13.2	32	2200	10.7	8.6

In figure 10 the stiffness is plotted as a function of the mean stress level for the material with three different fine contents. As can be seen there stiffness decreases as the fine content of the material increases. This is in good agreement with the general knowledge that dense graded materials usually have the highest strength at fine contents below 9 % but the stiffness decreases as the fine content increases after that.

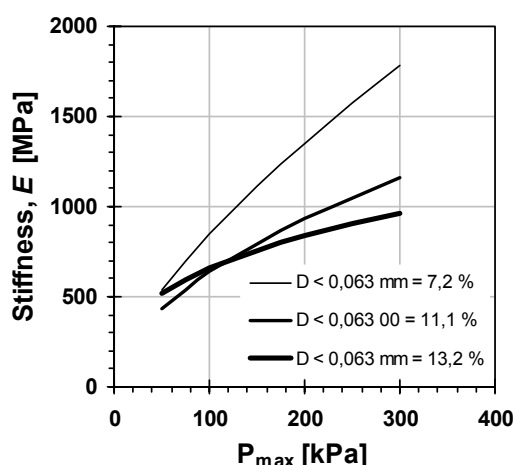


Figure 10. Stiffness as a function of the mean stress level for the Daelisa material with different contents of fines. All samples were compacted according to the Standard Proctor compaction method.

6 DISCUSSION

Based on this testing it can be stated that different compaction levels influenced the stiffness estimation. For some materials stiffness clearly increased as the compaction effort increased. Moisture also influenced the stiffness behaviour. As the moisture content increased, stiffness increased. This was true when the degree of saturation was well below full saturation. However as the moisture content started to increase and the degree of saturation neared full saturation, stiffness

was reduced, and in some cases a total collapse of the specimen occurred during the testing procedure. The reason for this could be a build-up of pore pressure in the specimen leading to a reduction of the effective stresses in the sample.

Stiffness has also been shown to be dependent on the contents of fines in the material. This is in good agreement with other findings that dense graded materials usually have the highest strength as the fine content is below approximately 9 % but decreases gradually as the fine content exceeds that value.

Other factors like different petrological composition, shape and surface characteristics of the grains does probably also affect the stiffness of the materials. These factors have not been studied so far, but ongoing research deals with this matter. However it seems to be that materials consisting of aggregates of high strength, like the Holabru material (strong, altered, dense basalt) tends to give higher stiffness values than materials consisting of aggregates of poorer quality, like the Daelisa material (weak, very altered, dense basalt), and that the difference in stiffness is at least to some extent due to different petrological composition.

7 ACKNOWLEDGEMENTS

This research project was funded by the Icelandic Research Council and the research fund of the Public Roads Administration of Iceland.

8 REFERENCES

- AASHTO T 294-92 I. 1992. Interim method of test for resilient modulus of unbound granular base/subbase materials and subgrade soils – SHRP protocol P46. American Association of State Highway and Transportation Officials.
- Brown, S.F. 1996. Soil mechanics in pavement engineering. *Geotechnique* 46(3): 382-426.
- CEN prENV 00227413. 1997. Unbound and hydraulic bound mixtures for roads – Test methods – Cyclic load triaxial test. Draft. Brussels: CEN/TC227/WG4/TG2, 18 p.
- Erlingsson, S. 2000. Dynamic triaxial testing of unbound base course materials. *Proceedings of the XIII Nordic Geotechnical Conference, NGM 2000*: 69-76. Finnish Geotechnical Society, Helsinki.
- Erlingsson, S. & Magnúsdóttir, B. 2002. Dynamic triaxial testing of unbound granular base course materials, *Proceedings of the 6th International Conference on the Bearing Capacity of Roads and Airfields*, Lisbon, Vol 2: 989-1000. A.A. Balkema Publishers.
- Gomes-Correia, G., Hornych, P & Akou, Y. 1999. Review of models and modelling of unbound granular materials. In G. Gomes-Correia (ed.), *Proceedings of an international workshop on modelling and advanced testing for unbound granular materials*: 3-15. Lisbon: Balkema.